Pattern Evocation and Energy-Momentum Integration of the Double Spherical Pendulum

by

Jeffrey M. Wendlandt

B.S.M.E. (University of Illinois at Champaign-Urbana) 1991
M.S.M.E. (University of California at Berkeley) 1993

A thesis submitted in partial satisfaction of the
requirements for the degree of
Master of Arts

in

Mathematics

in the

GRADUATE DIVISION
of the
UNVIERSITY of CALIFORNIA at BERKELEY

Committee in charge:

Professor Jerrold E. Marsden, Chair
Professor S. Shankar Sastry
Professor Alan D. Weinstein

Abstract

This thesis explores pattern evocation and energy-momentum integration of the double spherical pendulum. Pattern evocation is a phenomenon where patterns emerge when the flow of a dynamical system is viewed in a frame that rotates relative to the inertial frame. Energy-momentum integration integrates the equations of motion and exactly preserves energy and momentum at each time step. The thesis begins with a summary of the theory on pattern evocation for Hamiltonian systems with symmetry. The result of this theory is that if the motion in the reduced space is periodic, quasiperiodic, or almost periodic, respectively, then in a suitably chosen rotating frame with constant velocity, the motion in the unreduced space is also periodic, quasiperiodic, or almost periodic, respectively. The motion in this rotating frame may have a particular pattern or symmetry. Examples of this theory are demonstrated for the double spherical pendulum. A differential-algebraic model is created for the double spherical pendulum and is integrated with a publically available simulation package called MEXX. This simulation technique is described followed by a description of an energy-momentum integrator. The thesis concludes with a comparison of the energy-momentum integrator and the MEXX simulation.

Contents

1 Introduction

This thesis is an exploration of pattern evocation in the double spherical pendulum (DSP) and also examines an integration method of the DSP that preserves both energy and momentum. Patterns have been discovered in Hamiltonian systems when the flow of the system is viewed in a rotating frame. This was studied for point vortices in [Kunin et al., 1992]. A goal in [Marsden and Scheurle, 1995] is to develop theory for this phenomenon. This thesis provides a summary of the theory and demonstrates the pattern evocation phenomenon in the double spherical pendulum. This thesis also develops an energy-momentum integrator that exactly preserves both the angular momentum about the vertical axis and the energy. The energy-momentum integrator is compared to a differential-algebraic equation solver for multibody systems called MEXX. This work suggests that energy-momentum integrators may provide simulation results quickly at reasonable accuracy.

A summary of the theory in [Marsden and Scheurle, 1995] is presented in the first section of the thesis. The next section describes the simulation and visualization method used to search for the patterns in the DSP simulation data. The following section presents the simulation results and describes three examples of pattern evocation. An energy-momentum integrator is created for this thesis work and is described in the

next section. This section concludes by comparing the results from the energy-momentum integrator and the MEXX simulation. Part of the work presented in this thesis is published in [Marsden et al., 1995].

2 Summary of Theory on Pattern Evocation

A summary of some of the theory in [Marsden and Scheurle, 1995] is presented in this section. A result of this paper is that if there is a fixed point, a periodic orbit, a quasiperiodic orbit, or an almost periodic orbit, respectively, in the reduced space, then in a suitably chosen moving frame with *constant* velocity, the motion is also fixed, periodic, quasiperiodic, or almost periodic, respectively, in the unreduced space. The paper also describes how discrete symmetries play a role in the visualized orbits and the reduced orbits.

A summary of some aspects of reduction is presented here. A more detailed background is contained in [Marsden and Ratiu, 1994], [Abraham and Marsden, 1978], and [Marsden, 1992]. Let G be a Lie group acting on a manifold M. Let X be a vector field that is $G-$invariant. The flow of X produces a one parameter group of transformations, $F_t : M \to M$. There is a reduced flow, $\phi_t : M/G \to M/G$ on the orbit space, M/G. In this case, $\pi \circ F_t = \phi_t \circ \pi$, where $\pi : M \to M/G$ is the projection of the manifold to the orbit space. A fixed point, $s \in M/G$, corresponds to periodic orbit in $\pi^{-1}(s)$ and a point in $\pi^{-1}(s)$ is called a *relative equilibrium*. If there is a periodic orbit in the reduced space, the corresponding motion in the unreduced space is called a *relative periodic orbit*. The trajectory through a relative equilibrium, $z_0 \in M$, is given by

$$z(t) = \exp(t\xi)z_0$$

for some $\xi \in \mathfrak{g}$, the Lie algebra of G. Viewing the motion of the relative equilibrium in a moving frame with velocity ξ means that we replace $z(t)$ by $\exp(-\xi t)z(t)$. In this frame, the motion appears to be fixed. A similar notion is true for periodic and quasiperiodic motions in the orbit space.

Theorem 1 *Assume that the exponential map* $\exp : \mathfrak{g} \to G$ *is surjective. Assume that* $c(t)$ *is a relative periodic orbit and denote the period of the flow in the reduced orbit by* T*. Then there is a Lie algebra element* $\xi \in \mathfrak{g}$ *such that* $\exp(-\xi t)c(t)$ *is also periodic with period* T*.*

A similar theorem exists for symplectic reduction. Let P be a symplectic manifold and G a Lie group acting on P. Let $\mathbf{J} : P \to \mathfrak{g}^*$ be an Ad*-equivariant momentum map. For a fixed value μ of $\mathbf{J}$, let $G_\mu = \{g \in G | \mathrm{Ad}^*_{g^{-1}} \cdot \mu = \mu\}$ be the isotropy subgroup of G with Lie algebra $\mathfrak{g}_\mu$. The symplectic reduced space is $P_\mu = \mathbf{J}^{-1}(\mu)/G_\mu$.

Theorem 2 *Assume that the exponential map* $\exp : \mathfrak{g}_\mu \to G_\mu$ *is surjective. Assume that* $c(t)$ *is a relative periodic orbit and denote the period of the flow in the reduced orbit by* T*. Then there is a Lie algebra element* $\xi \in \mathfrak{g}_\mu$ *such that* $\exp(-\xi t)c(t)$ *is also periodic with period* T*.*

This value of ξ in the previous theorems is called the *critical velocity*. An explicit formula for the critical velocity is provided in the paper for systems with cyclic coordinates. For a Lagrangian, $L(x, \dot{x}, \dot{\theta})$, θ is a cyclic coordinate and we look at a Lagrangian of the form kinetic energy minus potential energy:

$$L(x, \dot{x}, \dot{\theta}) = \frac{1}{2} g_{\alpha\beta}\dot{x}^\alpha \dot{x}^\beta + g_{a\beta}\dot{\theta}^a \dot{x}^\beta + \frac{1}{2} g_{ab}\dot{\theta}^a \dot{\theta}^b - V(x), \tag{2.1}$$

where g_{ab} are the components of the mass matrix, and $V(x)$ is the potential energy. The locked inertia tensor, $\mathbb{I} : \mathfrak{g} \to \mathfrak{g}^*$, is given by

$$< \mathbb{I}\eta, \zeta > = \ll \eta_Q, \zeta_Q \gg,$$

where $\eta, \zeta \in \mathfrak{g}$, η_Q is the infinitesimal generator of the Lie algebra on the configuration manifold, Q, $< \cdot, \cdot >$ is the pairing of the Lie algebra and its dual, and $\ll \cdot, \cdot \gg$ is the kinetic energy metric. In the cyclic case, the components of the locked inertia tensor are $\mathbb{I}_{ab} = g_{ab}$, and the reduced trajectory is given by $x(t)$.

Theorem 3 *Suppose that $q(t) = (x(t), \theta(t))$ is a solution of the Euler-Lagrange equations on Q and that the reduced trajectory $x(t)$ is periodic with period T. Then relative to the frame with angular velocity given by*

$$\xi^a = \frac{1}{T}\int_0^T \mathbb{I}^{ca}(x(t))\mu_c dt - \frac{1}{T}\int_0^T g_{\alpha c}(x(t))\dot{x}^\alpha(t)\mathbb{I}^{ca}(x(t))dt \tag{2.2}$$

the solution $q(t)$ is also periodic with period T.

A function, $x(t)$, is *quasiperiodic* if $x(t) = \phi(\omega_1 t, \omega_2 t, ..., \omega_n t)$ for some function ϕ that is 2π periodic in all of its arguments and for some finite number of frequencies, ω_1 to ω_n. The following Theorem relates quasiperiodic motion in the reduced space to a suitably transformed motion in unreduced space.

Theorem 4 *Suppose that $q(t)$ is a solution of the Euler-Lagrange equations on Q and that the reduced trajectory is quasiperiodic with the frequencies $\omega_1, ..., \omega_n$ such that the following nonresonance condition is satisfied:*

$$\left|\sum_{k=1}^{n} j_k\omega_k\right| \geq \gamma \parallel j \parallel_{,}^{-\tau} \tag{2.3}$$

where γ and τ are positive constants and the norm is any convenient norm on n-space. Assume that the kinetic and potential energy functions are C^k for $k \geq \tau + 2$. Then, relative to a frame with the angular velocity given by the formula

$$\xi^a = \lim_{T\to\infty}\frac{1}{T}\int_0^T \left[\mathbb{I}^{ca}(x(t))\mu_c - g_{\alpha c}(x(t))\dot{x}^\alpha(t)\mathbb{I}^{ca}(x(t))\right] dt \tag{2.4}$$

the solution $q(t)$ is also quasiperiodic with the frequencies $\omega_1, ..., \omega_n$.

A similar result holds for almost periodic functions. A function, $f(t)$, is *almost periodic* if given any $\epsilon > 0$, there is a positive real number $T = T(\epsilon)$ such that any interval of length T on the real axis contains a number τ with $|f(t+\tau) - f(t)| \leq \epsilon$ for all $t \in \mathbb{R}$.

The role of discrete symmetries in pattern evocation is now discussed. Discrete symmetries may exist in a particular problem and may pass down to discrete symmetries in the reduced space. We now discuss how a discrete symmetry in a trajectory in the reduced space is visualized in the original space.

Let (P, Ω) be a symplectic manifold with a Lie group, G, acting on P. Let $\mathbf{J} : P \to \mathfrak{g}^*$ be an Ad*-equivariant momentum map for the action of G. The discrete group is denoted by Σ. We assume that Σ acts on G by group homomorphisms and denote the action by $\sigma_G : G \to G$. We also assume that Σ acts on P by symplectic or antisymplectic transformations and denote the action by $\sigma_P : P \to P$. Antisymplectic transformations change the sign of the symplectic form. Σ is composed of elements that correspond to symplectic transformations, $\Sigma_s \subset \Sigma$, and antisymplectic transformations, $\Sigma_a \subset \Sigma$. Let $\sigma_{\mathfrak{g}} : \mathfrak{g} \to \mathfrak{g}$ be the Lie algebra homomorphism created from taking the derivative of σ_G at the identity. Let $\sigma_{\mathfrak{g}^*} : \mathfrak{g}^* \to \mathfrak{g}^*$ be the dual of $(\sigma^{-1})_{\mathfrak{g}}$.

We now make several assumptions that guarantee that the discrete symmetries have a well defined action on the symplectic reduced space.

Assumption 1 *The actions of G and Σ are compatible in the sense that the following equation holds:*

$$\sigma_P \circ g_P = [\sigma_G(g)]_P \circ \sigma_P \tag{2.5}$$

This assumption implies that Σ has a well defined action on P/G. If $G = SO(2)$ and Σ is the group of reflections in vertical planes, then $\sigma_G(g)$ is conjugation, *i.e.*, $\sigma g \sigma^{-1} \in G$. Differentiating Equation (2.5) in the direction of $\xi \in \mathfrak{g}$ and comparing the resulting Hamiltonian vector fields reveals that

$$\mathbf{J} \circ \sigma_P = \pm\sigma_{\mathfrak{g}^*} \circ \mathbf{J} + (\text{cocycle}). \tag{2.6}$$

The paper assumes that the cocycle is zero and this leads to the following assumption.

Assumption 2 *The following equation holds:*

$$\mathbf{J} \circ \sigma_P = \pm \sigma_{\mathfrak{g}^*} \circ \mathbf{J} \tag{2.7}$$

where the plus sign is used for $\sigma \in \Sigma_s$ and the minus sign is used for $\sigma \in \Sigma_a$.

Assumption 1, Assumption 2, and the additional assumption that σ_P preserves the momentum map implies that Σ has a well defined action on the symplectic reduced space.

Let $w(t) \in P/G$ be a time dependent orbit and assume that it has the discrete symmetry $(\sigma_0, l_0) \in \Sigma \times \mathbb{R}$, where $\mathbb{R}$ acts by time shifts, *i.e.*,

$$\sigma_0 w(\pm(t - l_0)) = w(t) \tag{2.8}$$

for all time. The plus sign corresponds to symplectic transformations and the minus sign corresponds to antisymplectic transformations. Let $c(t)$ be an orbit that projects to $w(t)$ and let

$$\tilde{c}(t) = \exp(-\xi t) c(t) \tag{2.9}$$

be the transformed data in a rotating frame with velocity ξ. It is shown in their paper that

$$\sigma_0 \tilde{c}(\pm(t - l_0)) = g_0 \tilde{c}(t) \tag{2.10}$$

holds for some $g_0 \in G$ and for all $t \in \mathbb{R}$ provided that the momentum map, $\mathbf{J}$, is σ_0-invariant. We then seek a $g_1 \in G$ such that

$$\sigma_0 g_1 \tilde{c}(\pm(t - l_0)) = g_1 \tilde{c}(t), \tag{2.11}$$

or equivalently,

$$g_1^{-1} \sigma_0 g_1 \tilde{c}(\pm(t - l_0)) = \tilde{c}(t). \tag{2.12}$$

This last equation shows that $\tilde{c}(t)$ has the discrete symmetry $(g_1^{-1}\sigma_0 g_1, l_0)$. If $G = SO(2)$ and Σ is the group of reflections in vertical planes, then $g_1^{-1}\sigma_0 g_1$ is a reflection in a plane rotated by g_1^{-1}. Using Equation (2.10) and Equation (2.12), it can be shown that such a g_1 exists if there is a g_1 that solves the following equation:

$$\sigma_0 g_1^{-1} \sigma_0^{-1} g_1 = g_0. \tag{2.13}$$

In the case where $G = SO(2)$ and Σ is the group of reflections in vertical planes, g_1 is the square root of g_0.

The Double Spherical Pendulum (DSP) has two discrete symmetries: a reflection symmetry about vertical planes and a time reversal symmetry. Time reversal sends $t \mapsto -t$, $q_i \mapsto q_i$, and $\dot{q}_i \mapsto -\dot{q}_i$. The reflection symmetry is a symplectic transformation while the time reversal symmetry is an antisymplectic transformation. Both transformations change the sign of the momentum map so they do not provide a well defined action on the symplectic reduced space. If the actions of reversals and reflections are composed (order does not matter since they commute), then the momentum map is preserved and this combination of the discrete groups has a well defined action on the reduced space.

3 Simulation Technique

A differential algebraic equation (DAE) model of the Double Spherical Pendulum (DSP) is created. The DAE model enforces the length constraints in the DSP through Lagrange multipliers. In this section, we describe the publically available software, MEXX, for the simulation of multibody systems. The DAE model of the DSP is then presented followed by a description of the reduced variables for the DSP. The method of generating simulation results and graphing the data is then presented.

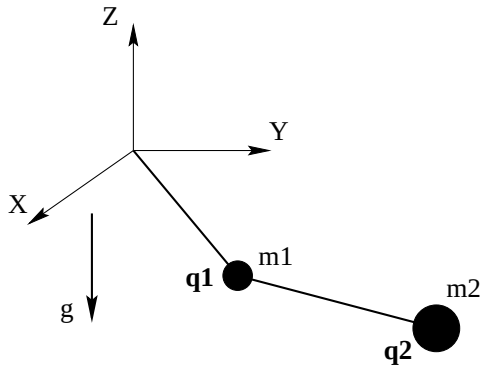

Figure 1: Double Spherical Pendulum

3.1 Summary of MEXX

MEXX is a multibody simulation package developed by Lubich, Engstler, Nowak, and Pöhle and described in [Lubrich et al., 1992]. MEXX is an acronym for MEXanical systems eXtrapolation integrator, and the program and documentation is available through anonymous ftp at elib.zib-berlin.de in pub/elib/codelib.

MEXX integrates nonstiff equations of motion for mechanical systems in the following form:

$$\begin{aligned} \dot{p} &= T(t,p)v && (3.1)\\ M(t,p)\dot{v} &= f(t,p,v,\lambda,u) - G(t,p)^T\lambda && (3.2)\\ 0 &= G(t,p)\cdot v + g^I(t,p) && (3.3)\\ \dot{u} &= d(t,p,v,\lambda,u), && (3.4) \end{aligned}$$

where $p(t)$ are the position variables, $v(t)$ are the velocity variables, $\lambda(t)$ are the Lagrange multipliers, and $u(t)$ are optional external dynamics. The length constraints are

$$0 = g(t,p). \tag{3.5}$$

The velocity constraints are contained in Equation (3.3).

The user needs to specify the initial conditions for the simulation, $p(t_0), v(t_0)$, and $u(t_0)$. External dynamics can include control inputs. The model presented in the next section for the DSP contains no external dynamics.

3.2 DAE Model of DSP

The DAE model of the DSP is described in this section and is shown in figure 1. The model fits the form presented in Equation (3.1)-(3.4) and there are no external dynamics. In the following equations for the DSP, m_i is the mass of the i'th point mass, q_i is the position vector for the i'th point mass, and l_i is the

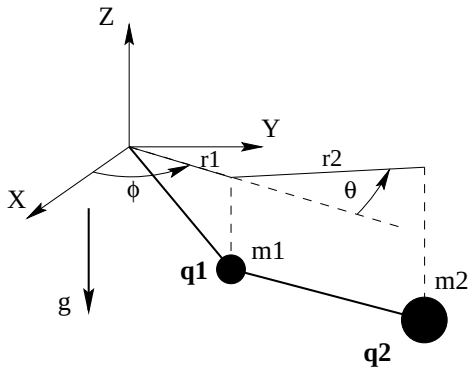

Figure 2: Reduced Coordinates for the Double Spherical Pendulum

length of the i'th segment:

$$M = \begin{bmatrix} m_1 I & 0 \\ 0 & m_2 I \end{bmatrix} \tag{3.6}$$

$$p = \begin{bmatrix} q_1 \\ q_2 \end{bmatrix} \tag{3.7}$$

$$v = \begin{bmatrix} \dot{q}_1 \\ \dot{q}_2 \end{bmatrix} \tag{3.8}$$

$$T = I \tag{3.9}$$

$$g = \begin{bmatrix} \frac{1}{2} q_1^T q_1 - \frac{1}{2} l_1^2 \\ \frac{1}{2}(q_2 - q_1)^T (q_2 - q_1) - \frac{1}{2} l_2^2 \end{bmatrix} \tag{3.10}$$

$$G = \begin{bmatrix} q_1^T & 0 \\ (q_1 - q_2)^T & (q_2 - q_1)^T \end{bmatrix} \tag{3.11}$$

$$f = \begin{bmatrix} 0 & 0 & -m_1 g & 0 & 0 & -m_2 g \end{bmatrix}^T \tag{3.12}$$

3.3 Reduced Variables

A choice of generalized coordinates are shown in Figure 2. The four coordinates, (r_1, r_2, θ, ϕ), are valid as long as one of the links do not line up with the z-axis. The action of the S^1 symmetry group only acts on the ϕ variable. Therefore, the reduced phase space is 6 dimensional and position coordinates on the reduced phase space are (r_1, r_2, θ).

3.4 Generating Simulation Results

A C-Program interfaces with the Fortran program MEXX to simulate the DSP. The C-Program contains the model definition and calls the MEXX integration routine. The simulation results are saved in a data file and loaded into Matlab or Mathematica to display the results. Matlab and Mathematica scripts display the data and transform the data to rotating frames. The velocity of the rotating frame is varied until the critical velocity is determined. Patterns at frame velocities not equal to the critical velocity have appeared in the simulations. These frame velocities are called *resonant velocities*. The position coordinates in the inertial frame are transformed to position coordinates in a frame with angular velocity, γ, by the following

equations:

$$\omega_\gamma = \begin{bmatrix} 0 \\ 0 \\ \gamma \end{bmatrix} \tag{3.13}$$

$$\hat{\omega}_\gamma = \begin{bmatrix} 0 & -\gamma & 0 \\ \gamma & 0 & 0 \\ 0 & 0 & 0 \end{bmatrix} \tag{3.14}$$

$$\begin{bmatrix} \tilde{q}_1(t) \\ \tilde{q}_2(t) \end{bmatrix} = \begin{bmatrix} e^{-\hat{\omega}_\gamma t} q_1(t) \\ e^{-\hat{\omega}_\gamma t} q_2(t) \end{bmatrix} \tag{3.15}$$

The new position data, $(\tilde{q}_1(t), \tilde{q}_2(t))$, is then graphed and reveals patterns for particular angular velocities and for particular initial conditions. The transformed data is the data as viewed in a camera looking down the z-axis that is rotating with angular velocity γ. Revealing patterns proceeds by choosing initial conditions, simulating, and viewing the data in moving frames. It is extremely helpful to make a movie of the position trajectories parameterized by the angular velocity. A particular example of a movie is seen in Figure 3. The first frame is in the upper left corner and the last frame is in the lower right corner. See also URL http://robotics.eecs.berkeley.edu/~wents/home_page.html for a MPEG movie file.

4 Simulation Results and Patterns

Several cases of pattern evocation in the DSP are demonstrated in this section. Each case corresponds to a different set of initial conditions. The first case does not appear to have a periodic motion in the reduced space but still reveals patterns for particular camera angular velocities. The second case has an orbit in the reduced space that resembles a periodic motion. In the third case, patterns appear and then vanish as the simulation time is increased. This last example has a discrete symmetry in the reduced space and this symmetry is visualized in particular moving frames. For each simulation, the trace of the two masses in an inertial frame is shown as well as the motion in the frame with critical angular velocity. Resonant patterns are then presented. Finally, the trajectories of the reduced position coordinates are shown. In the following simulations, $m_1 = 2.0$kg, $m_2 = 3.5$kg, $l_1 = 4.0$m, $l_2 = 3.0$m, and $g = 9.81$m/s^2.

4.1 Pattern I

In the first example, the initial conditions are $x_1 = 2.820$m, $y_1 = 0.025$m, $x_2 = 5.085$m, $y_2 = 0.105$m, $\dot{x}_1 = 3.381$m/s, $\dot{y}_1 = 2.506$m/s, $\dot{x}_2 = 2.497$m/s, and $\dot{y}_2 = 10.495$m/s. The position and velocity of the z-coordinate is determined from the constraints and the z-coordinate for both masses is taken to be negative. This motion results from a perturbation of a relative equilibrium. The initial conditions for the relative equilibrium are $x_1 = 3.0788$, $y_1 = 0.0$m, $x_2 = 5.5418$m, $y_2 = 0.0$m, $\dot{x}_1 = 0.0$m/s, $\dot{y}_1 = 4.8593$m/s, $\dot{x}_2 = 0.0$m/s, and $\dot{y}_2 = 8.7468$m/s.

The trajectory of the two masses in an inertial frame is shown in Figure 4(a). This motion projected onto the xy plane is shown in Figure 4(c). The motion in the frame with critical angular velocity is shown in Figure 4(b) and 4(d). In the critical velocity, the motion of the outer mass appears to move in a circular orbit while the inner mass moves in a star-like orbit. Notice the striking difference between Figure 4(a) and 4(b).

Four patterns are shown in Figure 5 which are denoted resonant patterns. The angular velocity of the frame is below the critical angular velocity in Figure 5(a)-(c) and above the critical angular velocity for Figure 5(d). The pattern in Figure 5(a) is an ellipse in the outer mass and an irregular ellipse for the inner mass. A trajectory resembling a triangle appears in the next pattern. This pattern has the discrete symmetries of D_3, the symmetries of a 3-sided polygon. A trajectory resembling a square is then revealed in the next pattern. This pattern has the D_4 discrete symmetry. The last resonant pattern resembles two reflected arcs with a D_2 symmetry.

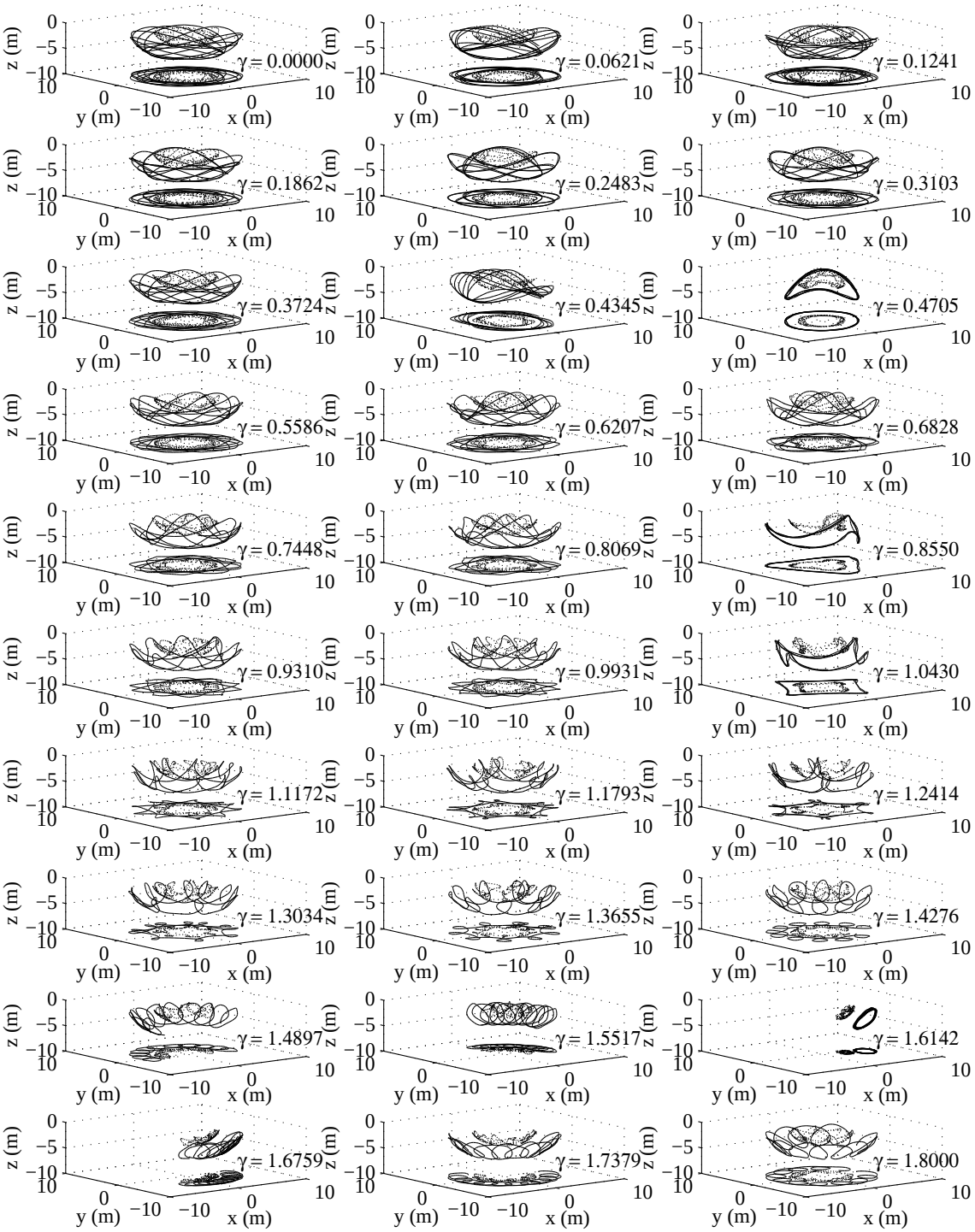

Figure 3: Movie Frames

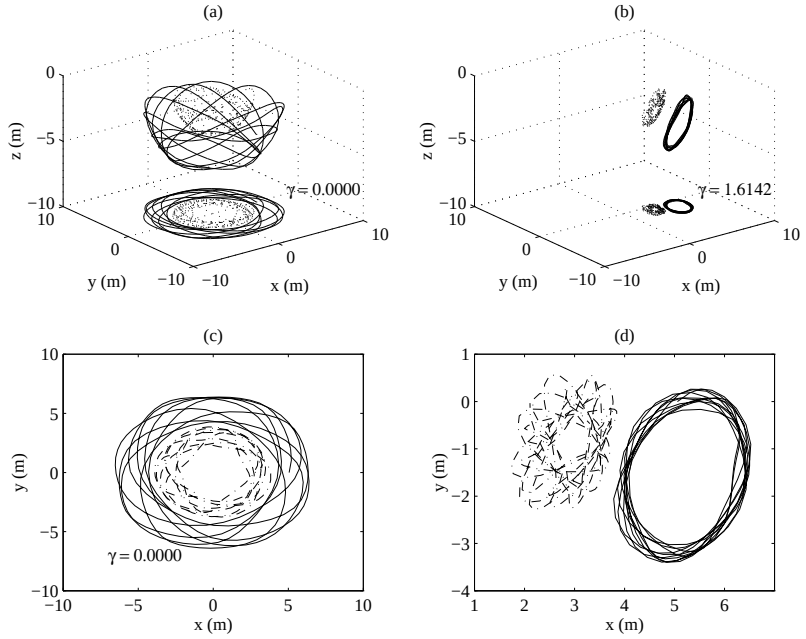

Figure 4: Trace of the two masses for pattern I: (a) inertial frame (b) critical angular velocity. Projection of the traces: (c) inertial frame (d) critical angular velocity

There appears to exist a relationship between the angular velocities that evoke a pattern, the critical angular velocity, and the discrete symmetry observed. Let γ_c be the critical angular velocity and γ_n be the angular velocity for the n-fold symmetry, D_n. Let F be the period in the reduced orbit. Then

$$|\gamma_c - \gamma_n| = \frac{m}{n}F, \tag{4.1}$$

where m and n are integers.

We now apply Equation (4.1) to the resonant patterns. A D_4 symmetry is shown in Figure 5(c) and the corresponding angular velocity is $\gamma_4 = 1.0403$rad/s. The critical angular velocity is $\gamma_c = 1.6142$rad/s. F is found to be 2.2848s using Equation (4.1). For the pattern in Figure 5(b), $\gamma_3 = 0.8550$rad/s and Equation (4.1) predicts that F is 2.2776s. The patterns in Figure 5(a) and 5(d) both have a D_2 symmetry group. For the pattern shown in Figure 5(a), the predicted value for F is 2.2874s, and for Figure 5(d), F is predicted to be 2.2876s. The largest difference between the calculated F's is 0.01s.

The motion in the reduced position coordinates is shown in Figure 6. Figure 6(a) is the trajectory of the three reduced position coordinates parameterized by time. Figure 6(b)-(d) are the projections onto the coordinate planes. There appears to be no periodic motion in Figure 6(a)-(d). Figure 6(b) appears to reveal trajectories that are evenly spaced and follow a similar trajectory.

Figure 7 shows the reduced coordinates versus time. The motion is not periodic but does have an oscillatory motion.

4.2 Pattern II

The initial conditions for this simulation resulted from varying the initial conditions of the two masses hanging straight down and at rest. The initial conditions are $x_1 = 0.012$m, $y_1 = 0.009$m, $x_2 = 0.505$, $y_2 = 0.510$m, $\dot{x}_1 = 0.210$m/s, $\dot{y}_1 = -0.040$m/s, $\dot{x}_2 = -0.477$m/s, and $\dot{y}_2 = 0.023$m/s.

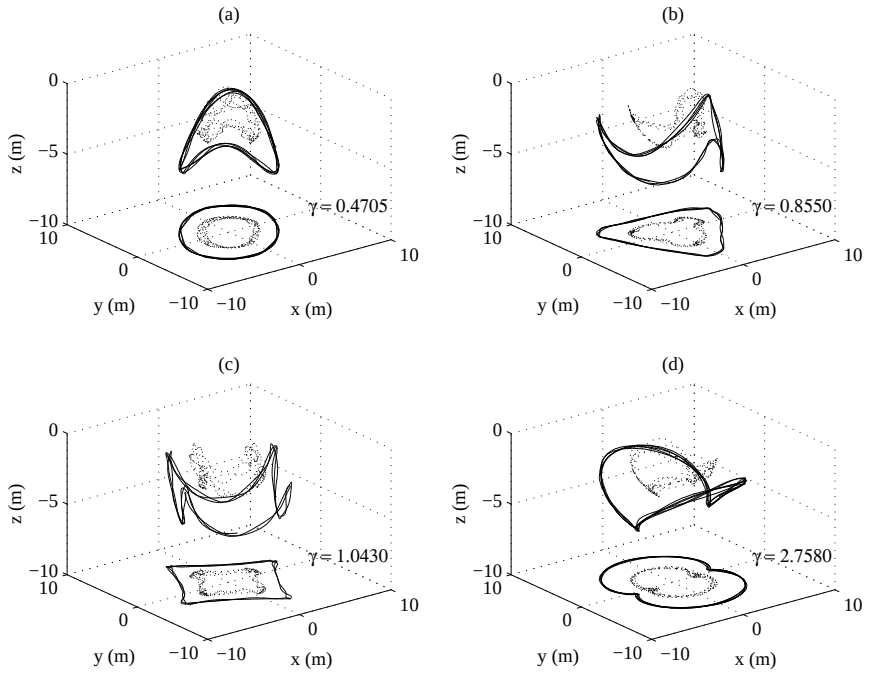

Figure 5: Resonant patterns for pattern I (a) $\gamma = 0.4705$ (b) $\gamma = 0.8550$ (c) $\gamma = 1.0430$ (d) $\gamma = 2.7580$

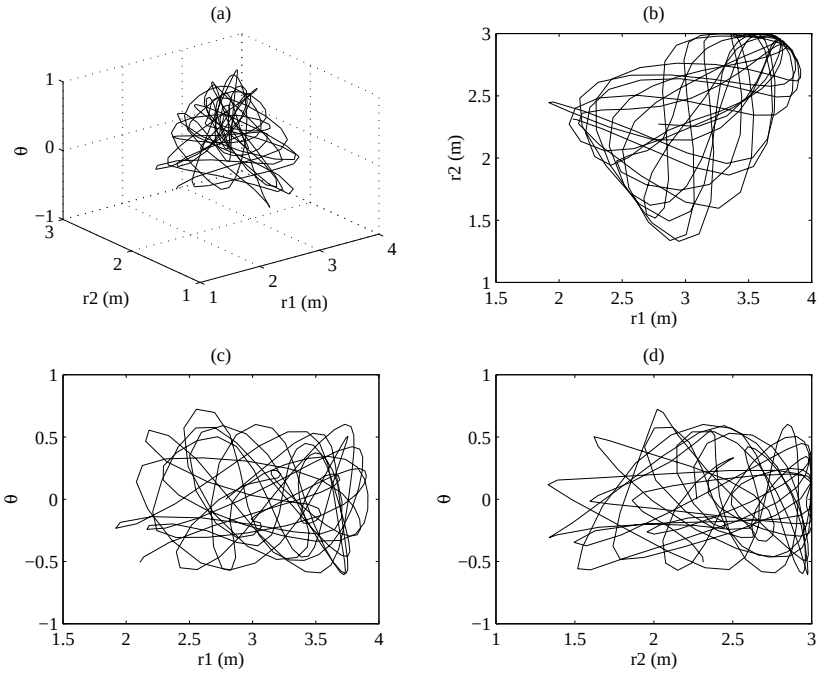

Figure 6: Reduced trajectories for pattern I: (a) θ-r_1-r_2 axes (b) r_1-r_2 axes (c) r_1-θ axes (d) r_2-θ axes

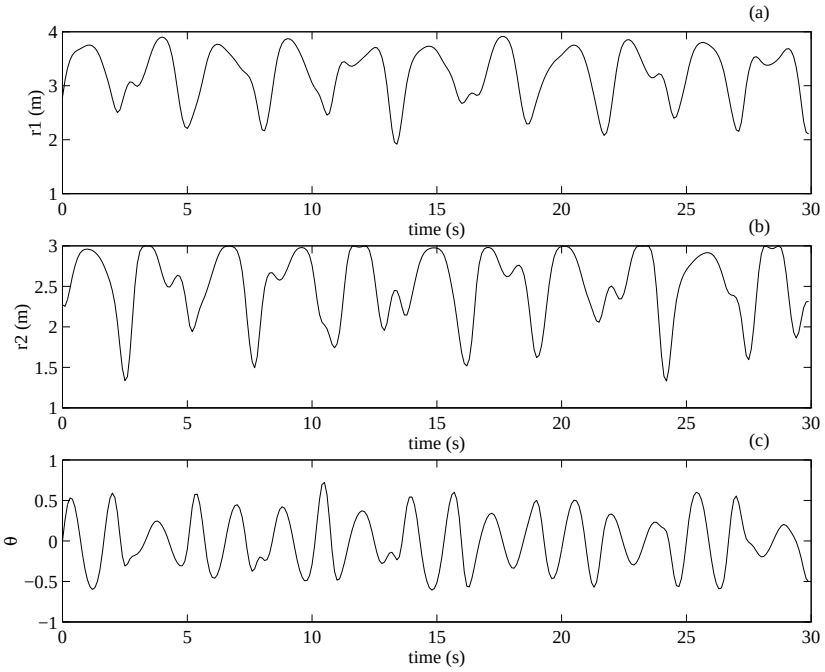

Figure 7: Reduced variables parameterized by time for pattern I

In Figure 8, the motion in the inertial frame and the frame with the critical angular velocity is shown. The motion in the critical frame shows the outer mass moving in a circular motion and the inner mass moving in a trajectory resembling a "figure eight". The critical angular velocity is $\gamma_c = 1.253$rad/s.

Figure 9 reveals four resonant patterns. Figure 9(a) and 9(b) result from angular velocities below γ_c and 9(c) and 9(d) result from angular velocities above γ_c. The pattern in Figure 9(a) and 9(c) have a D_3 symmetry. Figure 9(b) has a D_4 symmetry and Figure 9(d) has a D_2 symmetry.

The numerology discussed in the previous section seems to apply to this example as well. For the resonant pattern shown in Figure 9(a), the value of F calculated from Equation (4.1) is 2.493s. F is 2.512s for Figure 9(b), F is 2.493s for Figure 9(c), and F is 2.494s for Figure 9(d). The largest difference in the calculated F's is 0.019s.

The trajectories of the reduced position coordinates parameterized by time are shown in Figure 10. The trajectories resemble a periodic motion as seen in Figure 10(a)-(d).

The trajectories in the reduced position coordinates versus time are shown in Figure 11. Notice again that the motion resembles a periodic motion and the periodic pattern changes for each coordinate as time increases. Increasing a tolerance variable from 10^{-5} to 10^{-9} in the simulation reveals no apparent change in Figure 11.

4.3 Pattern III

The initial conditions for this simulation are $x_1 = 4.000$m, $y_1 = 0.000$m, $x_2 = 4.000$, $y_2 = 0.060$m, $\dot{x}_1 = -0.001$m/s, $\dot{y}_1 = 0.001$m/s, $\dot{x}_2 = 0.000$m/s, and $\dot{y}_2 = 6.000$m/s.

The motion in the inertial frame is shown in Figure 12(a) and 12(c). The motion as seen from the frame with the critical angular velocity, $\gamma_c = 1.4803$rad/s, is shown in Figure 12(b) and 12(d). The motion in Figure 12(d) resembles a set with a reflection symmetry about the x-axis.

Four resonant patterns are shown in Figure 13. A D_2 pattern is revealed in each of the patterns. The same discrete symmetry that is shown in the frame with critical angular velocity.

Equation (4.1) predicts values of F for this example as well. The period F is calculated to be 1.2283s

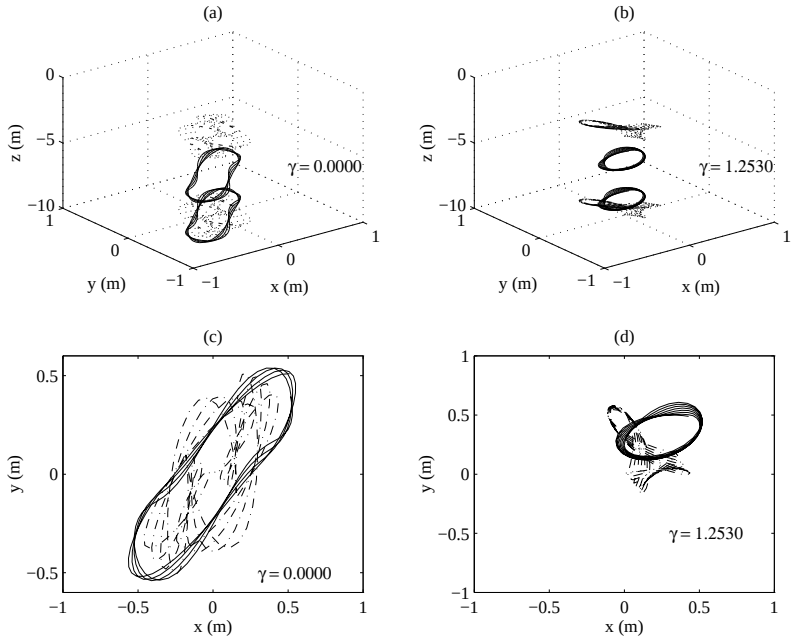

Figure 8: Trace of the two masses for pattern II: (a) inertial frame (b) critical angular velocity. Projection of the traces: (c) inertial frame (d) critical angular velocity

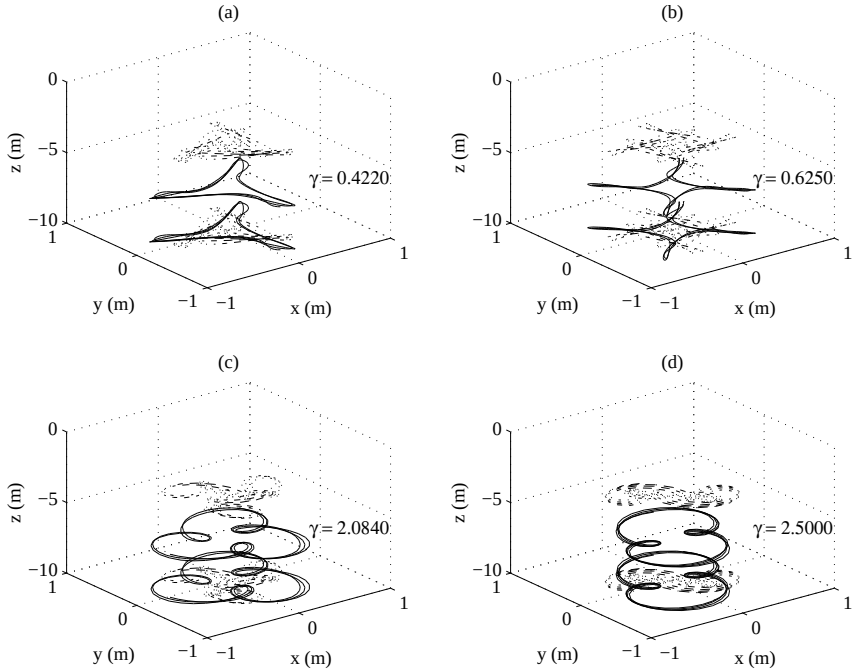

Figure 9: Resonant patterns for pattern II (a) $\gamma = 0.4220$ (b) $\gamma = 0.6250$ (c) $\gamma = 2.0840$ (d) $\gamma = 2.5000$

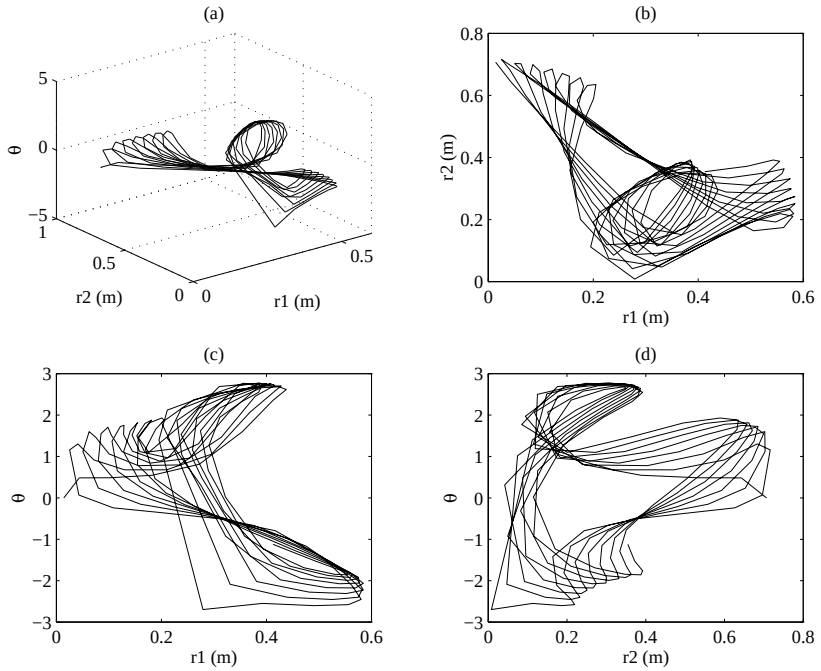

Figure 10: Reduced trajectories for pattern II: (a) θ-r_1-r_2 axes (b) r_1-r_2 axes (c) r_1-θ axes (d) r_2-θ axes

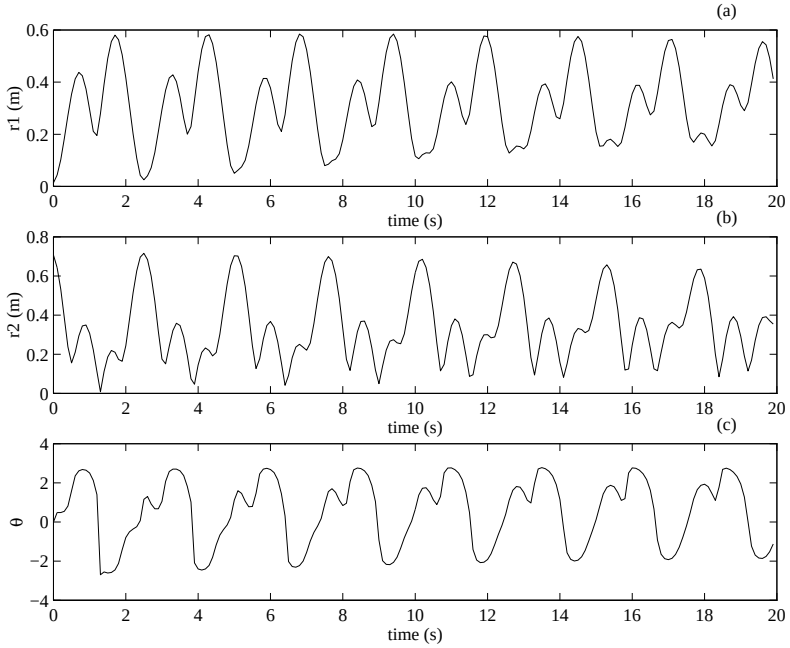

Figure 11: Reduced variables parameterized by time for pattern II

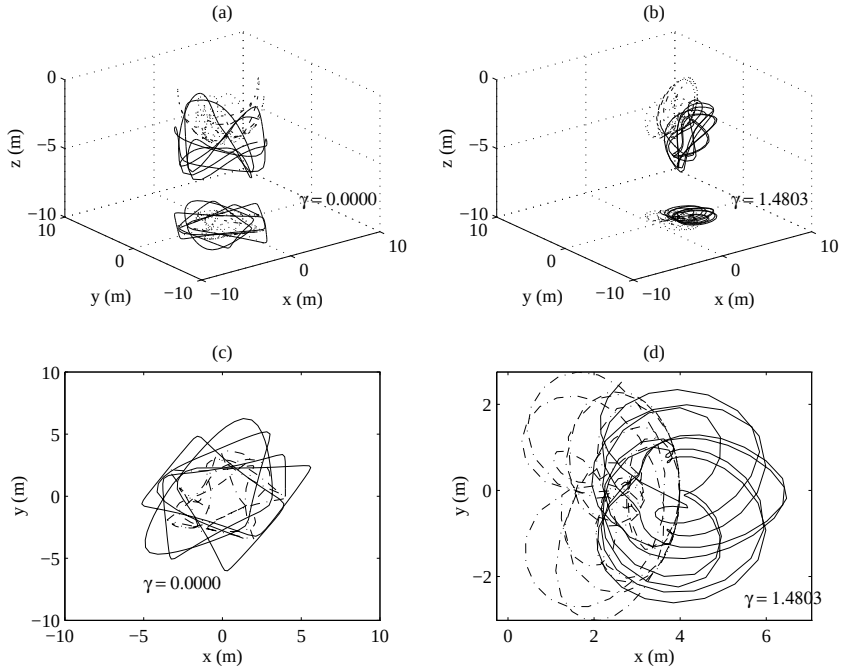

Figure 12: Trace of the two masses for Pattern III: (a) inertial frame (b) critical angular velocity. Projection of the traces: (c) inertial frame (d) critical angular velocity

for $\gamma_2 = 0.2520$rad/s with $m = 2$, 1.2316s for $\gamma_2 = 0.8645$rad/s with $m = 1$, 1.2154s for $\gamma_2 = 2.0880$rad/s with $m = 1$, and 1.2205s for $\gamma_2 = 3.3110$rad/s with $m = 3$. The calculated values of F vary from 1.2154s to 1.2316s with the average being 1.2240s.

In each of the four patterns shown in Figure 13, the pattern vanishes after simulating for longer times. The pattern still disappears if a MEXX tolerance variable is changed from 10^{-5} to 10^{-9}. The loss of the pattern is seen more readily in Figure 14 for $\gamma_2 = 0.8645$rad/s. The initial position is at $(x_2, y_2) = (4, 0)$ and the position of the second mass at $t = 20s$ is labeled in the figure. In this frame velocity, the trajectories of the masses cease to overlap after approximately 14s.

The trajectories of the reduced position coordinates parameterized by time are shown in Figure 15. The trajectories overlap in the beginning of the simulation, but the motion becomes irregular after simulating for longer times, $t > 14$s.

Trajectories for the reduced position coordinates versus time shown in Figure 16 appear to have the discrete symmetry of reflections and time reversals for a finite time interval. The following equations

$$\begin{aligned} r_1(t) &= r_1(-(t - 10.27)) \\ r_2(t) &= r_2(-(t - 10.27)) \\ \theta(t) &= -\theta(-(t - 10.27)) \end{aligned} \tag{4.2}$$

nearly hold for $0 \leq t \leq 5.135$. These equations correspond to a symmetry about the $t = 5.135s$ line shown in Figure 16. There also appears to be a symmetry of the same form about the $t = 10.27s$ line. This symmetry breaks down for t approximately greater than 14s. The discrete symmetry in the reduced space is seen in the unreduced space in Figure 12(d). The pattern has a reflection symmetry about the x-axis and it disappears for t approximately greater than 14s.

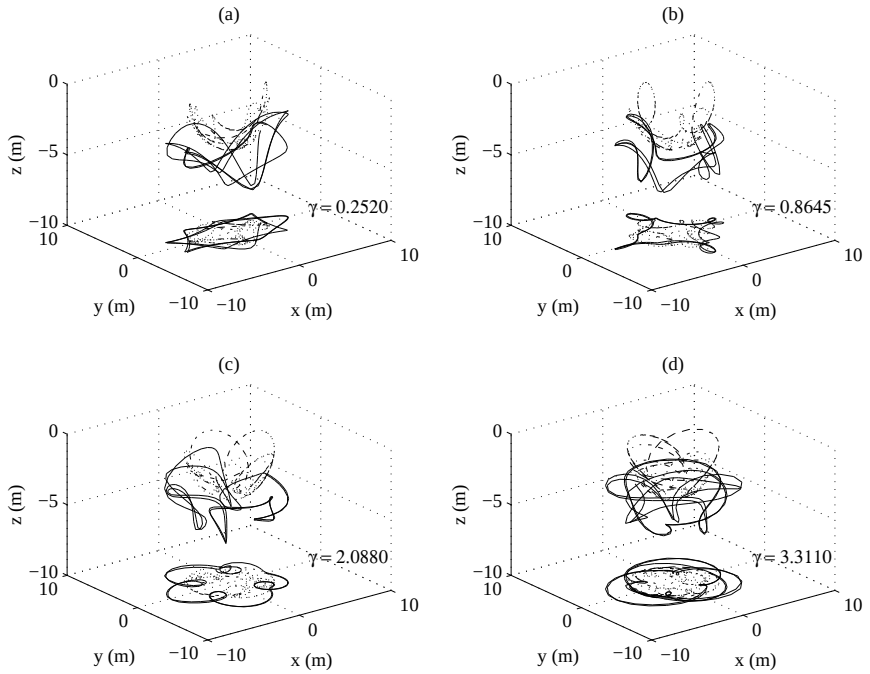

Figure 13: Resonant patterns for pattern III (a) $\gamma = 0.2520$ (b) $\gamma = 0.8645$ (c) $\gamma = 2.0880$ (d) $\gamma = 3.3110$

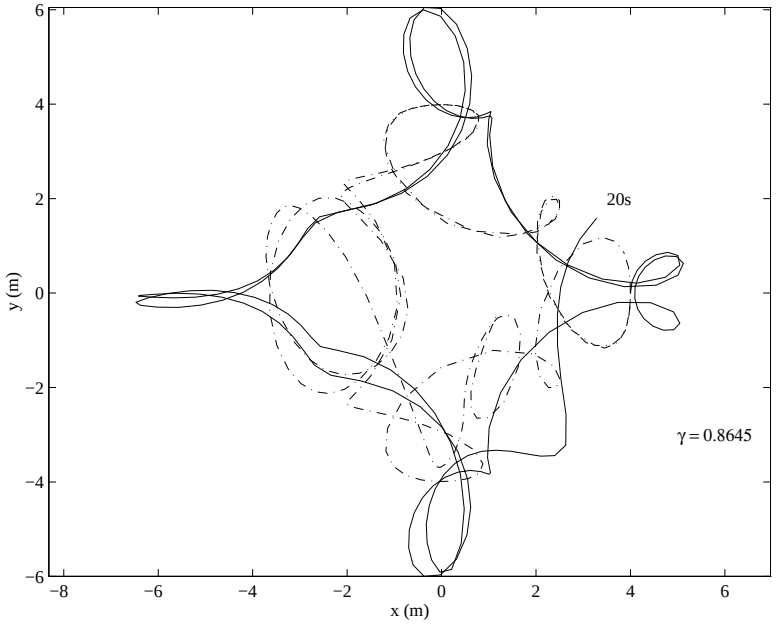

Figure 14: Resonant Pattern for pattern III, $\gamma = 0.8645$

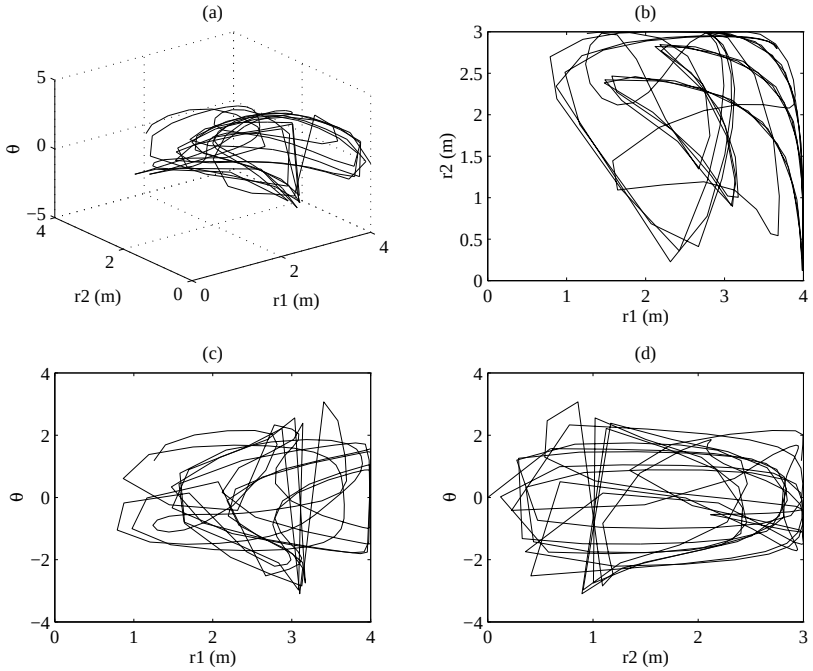

Figure 15: Reduced Trajectories for Pattern III: (a) θ-r_1-r_2 axes (b) r_1-r_2 axes (c) r_1-θ axes (d) r_2-θ axes

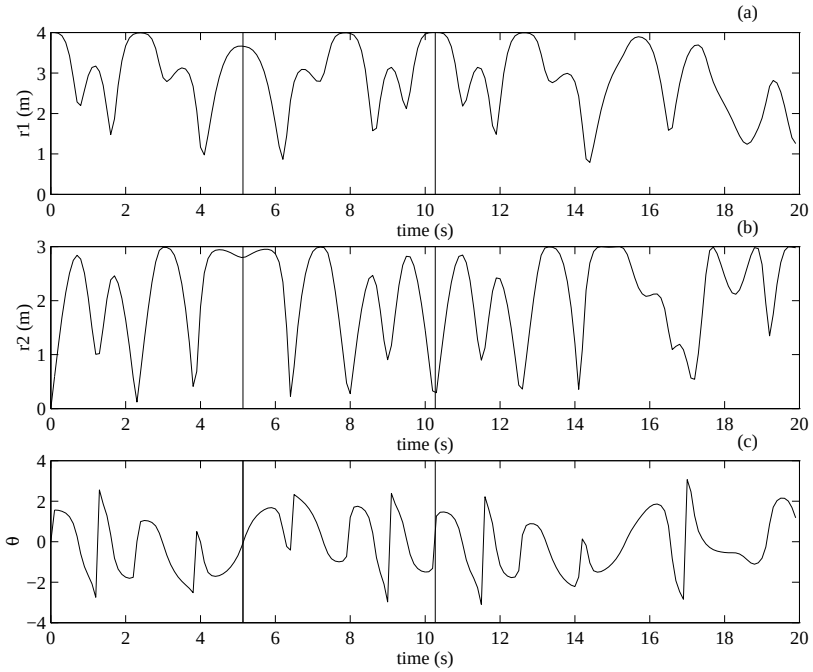

Figure 16: Reduced variables parameterized by time for Pattern III

5 Energy-Momentum Integrator

An energy-momentum integrator is presented in this section. These integrators preserve energy and momentum at each time step if the original continuous time dynamical system preserves energy and momentum. The algorithm was created after discussing the construction of energy-momentum integrators with Francisco Armero and Oscar Gonzalez. Oscar Gonzalez is currently finishing his Ph.D. thesis at Stanford and has proposed a method for constructing energy momentum integrators for mechanical systems that involve holonomic constraints. The following algorithm was constructed based on Oscar's general construction. Several useful references for energy-momentum integrators are [Gonzales and Simo, 1994], [Tarnow, 1993], [Simo and Gonzalez, 1993], and [Simo and Tarnow, 1992].

Oscar Gonzalez's general construction for energy-momentum integrators is briefly summarized in this section. The construction introduces a *discrete differential* which is analogous to the continuous differential. The defining properties of the *discrete differential*, $\mathbb{D}$, are

1. $\mathbb{D}_{(X,Y)}H \cdot (Y - X) = H(Y) - H(X)$ and
2. $\lim_{X \to Y} \mathbb{D}_{(X,Y)}H = D_Y H$,

where $X, Y \in P$, P is the linear phase space, $H : P \to \mathbb{R}$ is the original Hamiltonian, and $D_Y H$ is the normal differential of H evaluated at $Y \in P$ written as a column vector. The D's and $\mathbb{D}$'s presented here are column vectors. The *discrete differential* is a function of the current point in phase space and the point in phase space at the next time step. The *discrete differential* acts on functions and produces a column vector. The difference equation is determined from the following equation:

$$Z_{n+1} - Z_n = h\mathbb{X}_{(Z_n, Z_{n+1})}H = h\Omega^{\#}\mathbb{D}_{Z_n, Z_{n+1}}H, \tag{5.1}$$

where $\Omega^{\#}$ is the standard matrix such that the continuous Hamiltonian vector field is given by $\dot{z} = X_H(z) = \Omega^{\#} DH(z)$ and $h \in \mathbb{R}^+$ is the time step. A *discrete differential* in the standard position-momentum coordinates, (q, p), is used to generate the DSP algorithm equations and is given by

$$\mathbb{D}_{((q_1,p_1),(q_2,p_2))}H = \begin{bmatrix} \frac{\mathbb{D}^{(q)}|_{p_1}H \; + \; \mathbb{D}^{(q)}|_{p_2}H}{2} \\ \frac{\mathbb{D}^{(p)}|_{q_1}H \; + \; \mathbb{D}^{(p)}|_{q_2}H}{2} \end{bmatrix}, \tag{5.2}$$

where

$$\mathbb{D}^{(q)}|_{p_1}H = \left(I^{(q)} - n^{(q)}n^{(q)\,T}\right)\frac{\partial H}{\partial q}\left(\frac{q_1+q_2}{2}, \frac{p_1+p_2}{2}\right) + \frac{H(q_2,p_1) - H(q_1,p_1)}{\| q_2 - q_1 \|_2} n^{(q)}, \tag{5.3}$$

$n^{(q)} = \frac{q_2 - q_1}{\|q_2 - q_1\|_2}$, and $I^{(q)}$ is the identity matrix. The remaining three terms in Equation (5.2) are calculated analogously to Equation (5.3). The norms used in this section are two norms.

The *discrete differential* in (q, p) coordinates is applied to the following Hamiltonian with Lagrange multipliers for the DSP:

$$\begin{aligned} H(q,p,\lambda) = \frac{1}{2m_1} \| p_1 \|_2^2 + \frac{1}{2m_2} \| p_2 \|_2^2 + m_1 g q_{1,z} + m_2 g q_{2,z} + \\ \lambda_1 \left(\| q_1 \|_2^2 - l_1^2 \right) + \lambda_2 \left(\| q_2 - q_1 \|_2^2 - l_2^2 \right), \end{aligned} \tag{5.4}$$

where $q_{i,z}$ is the z coordinate of the ith point mass. Writing the constraints in the length squared form results in simpler algorithm equations.

Performing the calculations summarized above results in the following energy-momentum algorithm for

the DSP:

$$q_1^{n+1} - q_1^n - h\frac{1}{m_1}p_1^{n+\frac{1}{2}} = 0 \tag{5.5}$$

$$q_2^{n+1} - q_2^n - h\frac{1}{m_2}p_2^{n+\frac{1}{2}} = 0 \tag{5.6}$$

$$p^{n+1} - p^n + h\left[\begin{bmatrix} 0 \\ 0 \\ m_1 g \\ 0 \\ 0 \\ m_2 g \end{bmatrix} + \lambda_1 \begin{bmatrix} q_1^{n+1} + q_1^n \\ 0 \end{bmatrix} + \lambda_2 \begin{bmatrix} q_1^{n+1} + q_1^n - q_2^{n+1} - q_2^n \\ q_2^{n+1} + q_2^n - q_1^{n+1} - q_1^n \end{bmatrix}\right] = 0 \tag{5.7}$$

$$g_1^{n+1} \triangleq \left(q_1^{n+1}\right)^T \left(q_1^{n+1}\right) - l_1^2 = 0 \tag{5.8}$$

$$g_2^{n+1} \triangleq \left(q_2^{n+1} - q_1^{n+1}\right)^T \left(q_2^{n+1} - q_1^{n+1}\right) - l_2^2 = 0, \tag{5.9}$$

where q_i is the position vector for the ith mass, $p_i = m_i\dot{q}_i$ is the momentum for the ith mass, $p = [p_1^T p_2^T]^T$, q_i^n is the value of q_i at the nth time step, g_i^n is the ith length constraint at the nth time step, and $p_i^{n+\frac{1}{2}} = \frac{1}{2}(p_i^{n+1} + p_i^n)$.

The algorithm is an implicit integrator and requires the solution of nonlinear equations to determine p^{n+1}, q_1^{n+1}, q_2^{n+1}, λ_1, and λ_2 from q_1^n, q_2^n, p^n, and h. The function for p^{n+1} is calculated from Equation (5.7) and substituted into Equation (5.5) and (5.6). The resulting nonlinear equations do not involve p^{n+1} and are solved for q_1^{n+1}, q_2^{n+1}, λ_1, and λ_2. The solution is then used to calculate p^{n+1}. The initial conditions for the next step are updated and the algorithm proceeds to the next step.

By calculating

$$\frac{1}{m_1}p_1^{n+\frac{1}{2}} \cdot p_1^{\Delta} + \frac{1}{m_2}p_2^{n+\frac{1}{2}} \cdot p_2^{\Delta}, \tag{5.10}$$

where $p_i^{\Delta} = p_i^{n+1} - p_i^n$, using the algorithm equations and grinding through the algebra, you get that

$$K_{n+1} + V_{n+1} + \lambda_1 g_1^{n+1} + \lambda_2 g_2^{n+1} = K_n + V_n + \lambda_1 g_1^n + \lambda_2 g_2^n, \tag{5.11}$$

where

$$K_n = \frac{1}{2}\left(p^n\right)^T \begin{pmatrix} \frac{1}{m_1}I & 0 \\ 0 & \frac{1}{m_2}I \end{pmatrix} p^n$$

is the kinetic energy,

$$V_n = m_1 g q_{1,z}^n + m_2 g q_{2,z}^n$$

is the potential energy, and $q_{i,z}^n$ is the z-coordinate of the ith mass. Since the length constraints are satisfied at each time step, the algorithm preserves energy.

The following expression

$$q_1^{\Delta} \times p_1^{n+\frac{1}{2}} + q_1^{n+1} \times p_1^{\Delta} + q_2^{\Delta} \times p_2^{n+\frac{1}{2}} + q_2^{n+1} \times p_2^{\Delta} \tag{5.12}$$

equals $J^{n+1} - J^n$ where J^n is the angular momentum. This calculation reveals that the angular momentum about the z-axis remains constant while the momentum about the x-axis and the y-axis varies with time due to the force of gravity.

This algorithm is programmed in the C programming language, and the results are presented here. The graph of energy and momentum versus time for the energy-momentum integrator and the MEXX simulation is shown in Figure 17. The initial conditions for this simulation are the same as for pattern I

in Section 4.1. The momentum and energy remain constant over time for the energy-momentum integrator while the energy and momentum for the MEXX simulation decrease at an approximately linear rate. The accuracy of energy and momentum preservation depends on the solution accuracy of the nonlinear algorithm equations, Equations (5.5)-(5.9). The accuracy to which the nonlinear equations are solved is set by tolerance variables in the program.

We now attempt to compare the two simulation methods used to simulate the DSP. It is difficult to fairly compare these methods because there are many parameters in each integrator and it is not clear what parameters to use. The initial conditions used to compare the integration methods are the initial conditions used in Section 4.1 for pattern I. The reduced position coordinate, r_1, is then used to compare the simulation methods. A difference from a chosen standard is calculated and a measure of the difference is calculated. The measure of this difference is small between the MEXX simulation and an energy-momentum integration if we set h to be 0.001 in Equations (5.5)-(5.9). We therefore use the energy-momentum simulation at $h = 0.001$ as the standard. To measure the difference between simulations, we form a vector of r_1 over time and subtract the r_1 vector from the standard. We then take the 2-norm of the difference and divide by the number of elements in the vector. We denote the difference by e. For the energy-momentum simulations, $e = 1.42e-2$ for $h = 0.1$, $e = 2.7e-3$ for $h = 0.05$, $e = 4.924e-5$ for $h = 0.01$, and $e = 0.0$ by definition for $h = 0.001$. For the MEXX simulation, $e = 5.0522e-7$. A plot of r_1 versus time for the MEXX simulation and the energy-momentum simulation with $h = 0.001$ overlap and are indistinguishable. The trajectory of the r_1 variable produced from an energy-momentum simulation for $h = 0.001$ and for $h = 0.05$ is shown in Figure 18. The $h = 0.05$ simulation is a close approximation to the trajectory for $h = 0.001$. The MEXX simulation takes 9.6s on a Sparc 20 to simulate the DSP for 30s with these initial conditions. The energy-momentum integrator takes 12.84s with $h = 0.001$ and only 1.0s for $h = 0.05$. The energy-momentum integrator produces a reasonably accurate and fast simulation with $h = 0.05$.

This example leads one to speculate that the energy-momentum integrator may produce reasonably accurate results for relatively large step sizes. The large step sizes allow fast simulation times and this has applications in real-time simulation. It is desirable to simulate a complex multibody system with a real-time control system driving the inputs to the simulation. It is necessary that the simulations run fast enough to test the real-time control system. Also, fixed step size algorithms are often used so that one can guarantee that the simulation does not slow down for particular times [de Jalón and Bayo, 1994]. This can happen if an adaptive step size algorithm is used. Energy-momentum integrators may have applications in real-time simulation of multibody systems if they provide accurate results for large, fixed step sizes.

6 Conclusion

A background of the theory of pattern evocation in [Marsden and Scheurle, 1995] is presented in this thesis. The theory demonstrates an interaction between continuous groups, reduced phase spaces and discrete symmetries in the evocation of patterns. Several examples of pattern evocation in the double spherical pendulum are shown to demonstrate the theory. The examples do not satisfy the conditions of the theorems but still reveal interesting patterns. Future work in this example can be accomplished by calculating the values of ξ given by the formula and comparing these values to those determined through the simulation. The numerology equation can be explored more to determine the conditions under which it can be applied. It holds fairly well for the examples in this thesis.

This thesis also gives an example of energy-momentum integration of a holonomically constrained mechanical system. The results from this example lead one to speculate that fast, reasonably accurate simulations may be possible with these type of integrators. Future work involves energy-momentum integration in the presence of nonholonomic constraints as well as general constructions of energy-momentum integrators for multibody systems. Future work also involves finding energy-momentum integrators that have an order greater than two. The hope is that higher-order energy-momentum integrators provide greater efficiency than lower order methods.

I would like to thank several people who have helped me on this research. Jerry Marsden has given me valuable help and advice in this work. Oscar Gonzales and Francisco Armero have given me valuable

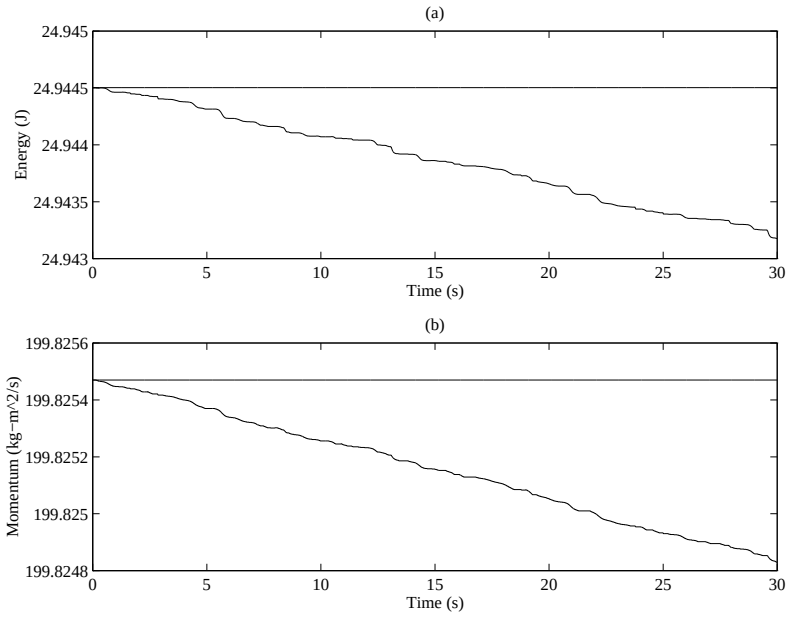

Figure 17: Energy and Momentum versus Time for Energy-Momentum Integrator and MEXX Simulation

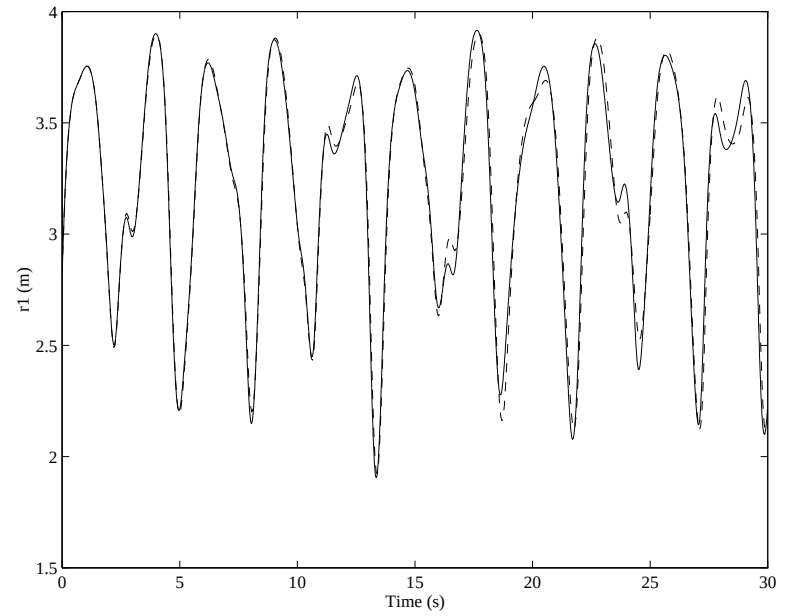

Figure 18: r_1 versus Time for Energy Momentum Integrator: $h = 0.05$(dashed), $h = 0.001$(solid)

help with energy-momentum integrators. Richard Murray and Abhi Jain have provided useful discussions on simulation techniques. I would like to thank my Ph.D. advisor, Shankar Sastry, for encouraging me and allowing me to do this research. I would also like to thank Alan Weinstein for being on my MA thesis committee. This research was partially supported by the Army Research Office under grant DAAL03-91-G0191 and by the National Institute of Health under grant R03RR06996 made to S. S. Sastry with the Electronics Research Laboratory.

References

[Abraham and Marsden, 1978] Abraham, R. and Marsden, J. (1978). *Foundations of Mechanics.* Addison-Wesley, Reading, Mass., second edition.

[de Jalón and Bayo, 1994] de Jalón, J. G. and Bayo, E. (1994). *Kinematic and Dynamic Simulation of Multibody Systems.* Springer-Verlag, New York.

[Gonzales and Simo, 1994] Gonzales, O. and Simo, J. (1994). On the stability of symplectic and energy-momentum algorithms for nonlinear hamiltonian systems with symmetry. preprint.

[Kunin et al., 1992] Kunin, I., Hussain, F., Zhou, X., and Prishepionok, S. (1992). Centroidal frames in dynamical systems i. point vortices. *Proc. Roy. Soc Lon.*, 439:441–463.

[Lubrich et al., 1992] Lubrich, C., Nowak, U., Pöhle, U., and Engstler, C. (1992). *MEXX - Numerical Software for the Integration of Constrained Mechanical Multibody Systems.* Konrad-Zuse-Zentrum für Informationstechnik Berlin (ZIB). Available through anonymous ftp at elib.zib-berlin.de in pub/elib/codelib.

[Marsden, 1992] Marsden, J. (1992). *London Mathematical Society Lecture Note Series 174: Lectures on Mechanics.* Cambridge University Press, Cambridge, England.

[Marsden and Ratiu, 1994] Marsden, J. and Ratiu, T. (1994). *Introduction to Mechanics and Symmetry.* Springer-Verlag, New York.

[Marsden and Scheurle, 1995] Marsden, J. and Scheurle, J. (1995). Pattern evocation and geometric phases in mechanical systems with symmetry. *Dynamics and Stability of Systems.* to appear.

[Marsden et al., 1995] Marsden, J., Scheurle, J., and Wendlandt, J. (July, 1995). Visualization of orbits and pattern evocation for the double spherical pendulum. In *Proceedings of the ICIAM Conference*, Hamburg.

[Simo and Gonzalez, 1993] Simo, J. and Gonzalez, O. (November 28 - December 3, 1993). Assessment of energy-momentum and symplectic schemes for stiff dynamical systems. In *ASME Winter Annual Meeting*, New Orleans.

[Simo and Tarnow, 1992] Simo, J. C. and Tarnow, N. (1992). The discrete energy-momentum method. conserving algorithms for nonlinear elastodynamics. *ZAMP*, 43:757–792.

[Tarnow, 1993] Tarnow, N. (July 1993). *Energy Momentum Conserving Algorithms for Hamiltonian Systems in the Nonlinear Dynamics of Solids.* PhD thesis, Stanford.